Interaction of walkers with a standing Faraday wave

Loïc Tadrist* and Tristan Gilet
Microfluidics Lab, Aerospace and Mechanical Engineering,
University of Liege, Allée de la découverte 9, 4000 Liège, Belgium
(Dated: May 12, 2026)

Walkers (i.e., bouncing droplets coupled to a local Faraday wave) are sent on an orthogonal standing wave. The trajectories of successive walkers form a straight-propagating beam towards the wave that splits into three distinct paths during the interaction with the wave. At the end of the interaction, walkers trajectories split again and are deviated in three main directions. The walkers trajectories show sensitivity to parameters and initial conditions but remain predictable in some regions of the parameter space. The dependence of the statistical distribution of deviations on the wave amplitude markedly differs from the prediction of quantum mechanics for a particle interacting with a standing electromagnetic wave.

I. INTRODUCTION

A vertically vibrated bath offers the possibility to observe long-living droplets at its surface. The vibration prevents coalescence by renewing the air cushion between the droplet and the bath at each period. Under more restrictive conditions, the coupling between a bouncing droplet and the standing waves that it generates triggers the horizontal motion (walking) of the droplet on the bath surface. These walkers, comprising both the droplet and the coupled underlying wave, have been presented as a potential hydrodynamic quantum analogue [1–4]. The borrowing of the adjective "quantum" is supported by convincing experiments that exhibit quantification of motion: quantized orbits in a well [5–8], eigenstates in a confined cavity [9–11] or quantified angular momentum [12, 13].

Nevertheless, the two iconic quantum mechanics experiments, namely two-slit diffraction and quantum entanglement, were not reproduced with walkers. The first attempts to create entanglement were made recently [14, 15]. The corresponding experiment positively shows that Bell inequalities can be violated by walkers because wave-mediated interactions do not allow to fulfill the assumptions of the theorem.

Many attempts were made to reproduce two-slit diffraction [16–18]. Originally, Couder and Fort [16] guided walkers towards a submerged linear obstacle glued at the bottom of the bath with two gaps as slits. They drew promising diffraction figures but the number of considered data points were too few to conclude [17]. Later, Andersen *et al.* [17] were unable to reproduce the observed diffraction pattern. By the time of those early works, experimental setups were subjected to external air currents that curved the trajectories of the walkers. Pucci *et al.* [18] performed a delicate air-tight experiment. They showed that walkers trajectories are mainly deviated by one of the two slits, sometimes with effects of the second slit. However, despite exhibiting peaks, the observed diffraction figure was different from that of quantum particles. Later, it was shown that diffraction was unlikely to occur with the experimental conditions considered by Pucci *et al.* [18], the length of the path through the second slit being larger than the damping length of the wavefield [19]. The most recent papers to date on the subject, [20, 21], improved the experimental capacity to produce diffraction by having larger damping lengths. Their findings support that diffraction occurs for walking droplets but that the diffraction figure is different from that of quantum mechanics in the parameter space explored. A major difference between the two systems is that the waves radiated by walkers do not exhibit similar amplitude in both slits, which prevents a quantum-like diffraction pattern. Wave amplitudes in both slits might be closer to each other with relativistic walkers [22].

Ellegaard and Levinsen [21] increased damping length by working extremely close to the Faraday threshold ($\gamma_F/(\gamma_F-\gamma)=1000$) which is difficult to master experimentally (any undesired temperature variation changes oil viscosity and drifts the Faraday threshold γ_F). An alternative would be to decrease the oil viscosity, although this would imply working with smaller droplets [23] which are more sensitive to air currents. The second experimental difficulty lies in the interaction between the capillary wave of the walker and the submerged obstacles which remains poorly characterized [24–26]. Therefore, with the existing experimental configuration, a quantum-like two-slit diffraction of walkers may not be achievable.

By contrast, the diffraction of a particle by a standing wave, known as Kapitza-Dirac diffraction [27–29] in quantum mechanics, is a configuration that does not involve interactions with obstacles. Gould *et al.* [30] provided first experimental evidence of this diffraction for sodium atoms interacting with a standing-wave laser field.

This configuration has recently been transposed to walkers by Primkulov *et al.* [31] : a beam of walkers crosses a pre-existing Faraday wave. The amplitude of the standing wave was reported to be of much higher amplitude (240 µm) than the typical wavefield generated by the walker itself (~ 10 µm). The reported experimental

* Also at Aix-Marseille Université, CNRS, ISM, Marseille, France; loic.tadrist@univ-amu.fr

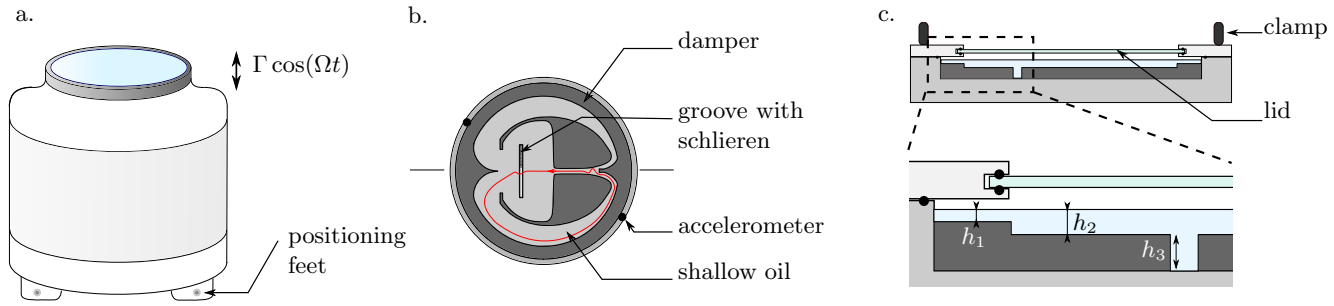

FIG. 1. Experimental set-up. a. An oil bath was placed on top of a shaker and positioned horizontally ($10\,\mu m\,m^{-1}$) thanks to positioning feet. b. Top view of the oil bath with a typical walker trajectory (red). Vibrations were recorded by a pair of accelerometers. Extremely shallow parts are indicated in dark gray, the experimental zone is indicated in light gray and groove in white. A synthetic Schlieren was placed in the groove for wave height measurement. c. Lateral view of the oil bath with h_1 =1.16 ± 0.02 mm, h_2 =2.16 mm and h_3=5 mm.

diffraction pattern is symmetric and made of four peaks, none of them corresponding to an absence of deviation. This diffraction pattern is reminiscent of the channeling of atoms interacting with an intense standing wave [32].

However, the interaction of atoms or electrons with a standing wave of light exhibits a variety of behaviors (including Bragg's scattering, channeling and diffraction), depending on both the wave intensity and the interaction time [28]. Are these behaviors also observed for walkers? Do walkers behave similarly to quantum particles when interacting with a standing wave?

In this paper, we report experimental data on the interaction of walking droplets with a weak to moderate standing wave ($0 < A < 9.5\,\mu m$). We analyze walkers trajectories and check their sensitivity to initial conditions and parameters. To test the analogy with quantum mechanics, we compute the dependence of the position and amplitude of the observed diffraction peaks on the amplitude of the standing wave.

II. EXPERIMENTAL SETUP

The experimental set-up is presented in figure 1. An oil reservoir of inner diameter 28 cm was placed on top of an electromagnetic shaker (V400LT, Data Physics) that generated a vertical acceleration $\Gamma\cos(\Omega t)$ of amplitude Γ and frequency $\Omega/2\pi$ =80 Hz. The shaker was initially leveled by 4 positioning feet. The residual inclination of the shaker platform was less than $10\,\mu m\,m^{-1}$ (figure 1a). The vertical acceleration of the shaker was measured thanks to two identical accelerometers placed at opposite positions on the sides of the reservoir. Accelerometers allowed first to check the uniformity and absence of distorsion of the vibration, and second to set acceleration limits to ensure shaker integrity.

Figure 1b shows the reservoir seen from above. A thin annulus (dark gray in Figure 1b) was submerged and glued inside the reservoir to damp capillary waves radiated by the meniscus at the reservoir edge. Two other pieces (also in dark gray in Figure 1b) were placed symmetrically within the annulus. Once the walker interacted with the standing wave, these pieces guided the walker back to its initial position. A typical trajectory is shown in red. The standing wave was generated in a groove of depth h_3 =5 mm oriented perpendicularly to the droplet trajectory. A synthetic schlieren was placed at the bottom of the groove to measure the topography of the Faraday wave therein. Any submerged obstacle was at least 55 mm away from the region of interaction.

The reservoir was made air-tight with a clamped lid (figure 1c). The liquid depth was h_2 =2.16 ± 0.02 mm and h_1 =1.16±0.02 mm in the over-damped regions (dark gray in Figure 1b). Liquid depth was measured at the beginning of each day of experiment with a manual caliper.

Both the bath and the droplet were made of silicone oil of viscosity 20 cSt (Sigma-Aldrich). The droplets were formed thanks to a 3D printed piezoelectric dispenser [33]. Once a droplet was formed, the lid was set back in place and clamped. Each droplet was used for several interaction experiments (from tens of minutes to few hours) until it finally coalesced with the bath.

During each interaction experiment, called trial, the walker was sent perpendicular to the groove, deviated by the standing wave therein with a diffraction angle θ, and automatically gathered back for a new test (figure 2a). See Supplemental Material for movies [34]. The bath was insulated from parasitic sunlight with opaque black curtains. Nevertheless, the recorded temperature in the oil bath (submerged K-type thermocouple) varied by more than 4 °C, subsequently inducing a variation of the oil viscosity and the Faraday acceleration threshold.

The shaker motion was controlled by a feedback loop similar to the one detailed in [35] but now aiming at maintaining the standing wave amplitude in the groove. A module implementing Lukas-Kanade tracking algorithm computed in real-time the gradient of the Faraday wave based on the synthetic Schlieren technique [36]. The standing Faraday wave amplitude was then estimated and the vibration amplitude was adjusted by PID feed-

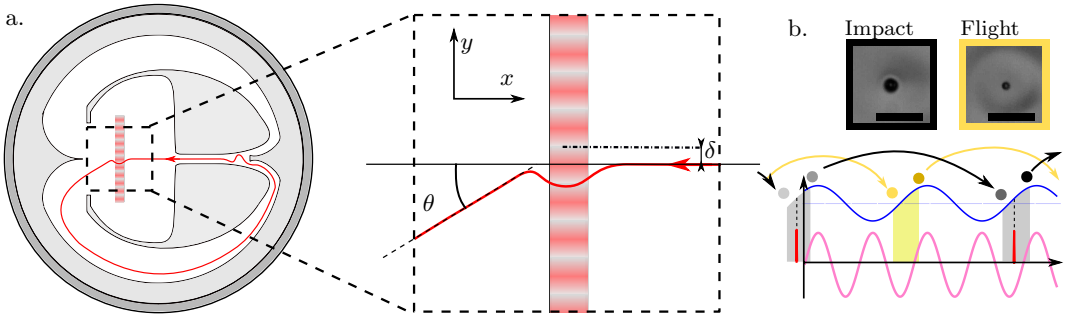

FIG. 2. Notations. a. Definition of distance δ and diffraction angle θ. The impact parameter is defined as the y-projected distance between the droplet incoming trajectory and the closest antinode of the Faraday wave in the groove (grey strips in the inset). b. Definition of impact (black) and flight states (yellow), in which the droplet can be at the instant of recording (red spike). The scale bar is 5 mm. Camera recording (red spike) is phase-shifted by $\pi/6$ with the shaker acceleration (pink). Faraday waves (blue) are phase-shifted by $\pi/4$ with respect to shaker acceleration.

back loop to maintain a targeted wave amplitude. This allowed to compensate for parasitic temperature variations. The feedback loop on the Faraday wave induces some variability because the vertical dynamics of walkers is slightly modified by the regulated driving acceleration. Mostly, the walker speed is slightly changed, which is then measured and taken into account. Nevertheless, we expect the system to be more reproducible with this feedback on the Faraday wave amplitude than with a control of the absolute acceleration γ.Targeted amplitudes were 1.9, 3.8, 5.8 and 7.7 µm. Actual Faraday wave amplitudes were recorded at the beginning of each trial.

Droplet positions were measured from top-view recordings at 20 Hz, synchronized with the bath to be able to decipher between flight and impact states (figure 2b). Droplet velocities and impact phases were post-treated with a custom Matlab script [37]. The initial walker speed v is defined as the median value of the droplet speed from the first 10 images, after the droplet gets out of the launching channel. The median value was chosen rather than the mean value to get rid off outlier points due to poor detection or unsaved images. The output angle is obtained by fitting a first order polynomial on the last 10 points of the droplet trajectory before it gets out of the camera view. The amplitude of the slope of Faraday waves was stored in memory along with its position on the image. Camera recorded pictures at a phase shift of $\pi/6$ with respect to the shaker acceleration. This phase shift allowed to distinguish clearly between flight and impact states (Fig. 2b). However, considering the $\pi/4$ phase shift between the Faraday waves and the shaker acceleration [19], measurements are corrected by a factor $1/\sin(\pi/12)$ to obtain the maximal wave amplitude. From these measurements, the distance δ is defined as the projected distance on the y-axis between the initial position (median of the first 10 points) and the position of the maximum of the wave gradient, see figure 2a. The impact parameter is then simply computed as $\phi = 2\pi\delta/\lambda_F$ where λ_F =4.75 mm is the Faraday wavelength in the groove. Impact phases of droplets initially recorded in flight state are shifted by π.

A cosine function of y was fitted on the measured gradient of the Faraday wave in the groove. A trial was discarded when the coefficient of determination of this fit was smaller than 0.9 or when multiple frames were missing due to a lag in the acquisition. The present data set gathers 3368 trials.

III. RESULTS

A. Diffraction figure of walkers

From the full dataset, walkers are sorted by velocity in two groups, low speed $v \in [11.5; 12.1]\text{mm s}^{-1}$ (1001 trials) and high speed $v \in [13.2; 13.8]\text{mm s}^{-1}$ (561 trials). The speed distribution and the standing wave amplitude distribution of the full dataset are given in supplementary material.

The trajectories are shown in figure 3a for low speed walkers and in figure 3b for high speed walkers. The initial beam of walkerss (from the right of the image) starts interacting with the groove at a distance $2\lambda_F$ and splits almost homogeneously. Then the beam of walkers is channeled into the three first antinodes of the standing wave ($y = \{-\lambda_F, 0, \lambda_F\}$). The paths split again after crossing the groove. At a distance, $2\lambda_F$ downstream of the groove, the trajectories become straight again. It indicates that interactions with either the groove or other submerged boundaries are negligible, and that there are no parasitic air currents.

When a walker interacts with the wave in the groove, the vertical bouncing dynamics of its droplet may be strongly perturbed, to the point where it shifts by one shaker period [37]. This event, called bouncing phase reversal, is witnessed as a switch between impact and flight state in the movies. The first occurrences of such shift during the interaction are represented in the insets of figures 3a and 3b. They are observed at a distance less than λ_F upstream of the groove.

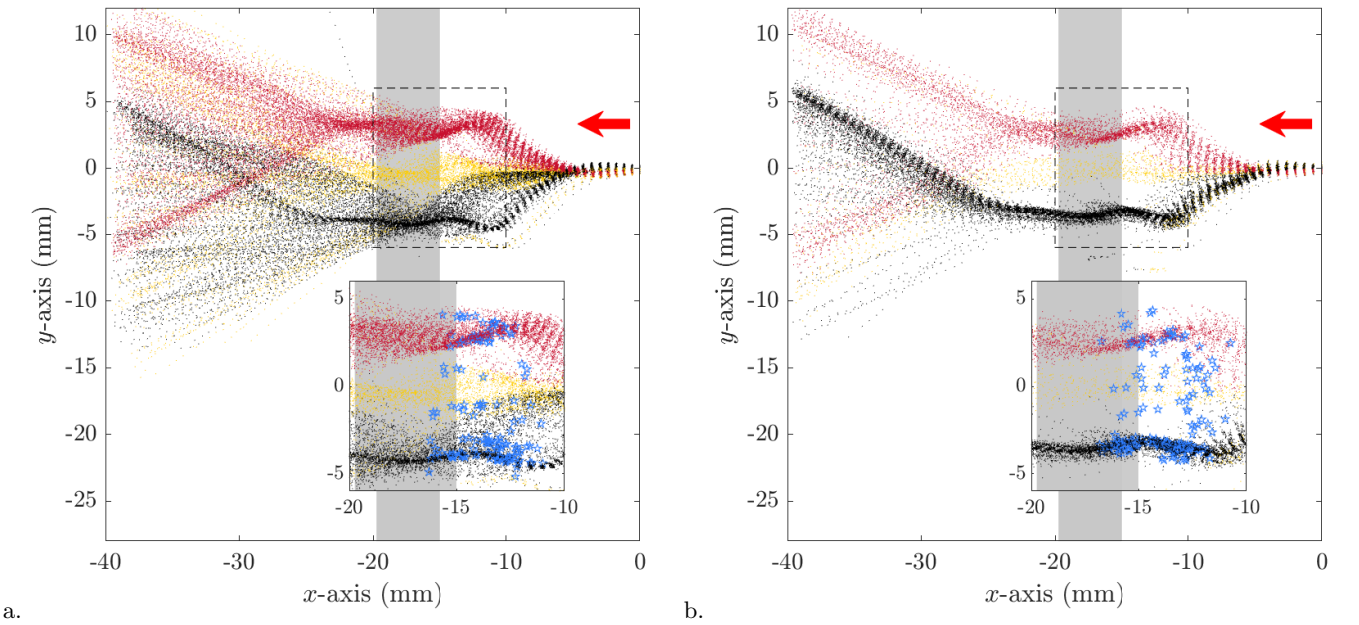

FIG. 3. Trajectories of walkers diffracted by a standing wave (gray shaded area) of amplitude $A \in [0; 9.5]$ µm. Trajectories are colored according to the crossed valley. Inset: Location of the first bouncing phase reversal (blue star) if any. a. Low-speed walkers. Velocity, $v \in [11.5; 12.1]\mathrm{mm\,s^{-1}}$. b. High speed walkers. Velocity, $v \in [13.2; 13.8]\mathrm{mm\,s^{-1}}$.

B. Predictability of experimental outcome

Walkers are sensitive to initial conditions and parameters. Among others their vertical dynamics is perturbed. The chosen valley (black red or yellow) is shown in the wave amplitude/impact parameter space of figure 4a for low speed walkers and figure 4b for high speed walkers.

To quantify this sensitivity, the parameter space is divided in cells of $0.5\,\mu\mathrm{m}\times\pi/3\,\mathrm{rad}$ (figure 4). The distribution of trials within the parameter space is not uniform, some regions gathering much more trials than others. This non-uniformity is a trace of the experimental set-up where (1) the impact parameter is not directly controlled, (2) the feedback-loop on wave amplitude is extremely delicate and has some hysteresis (3) the same droplet is used for multiple trials. To robustly analyze the sensitivity of the outcome to parameters, statistical significance of the outcome is tested with a 3-options combination model, one option corresponding to one valley.

In a given cell of the parameter space, $N = N_1 + N_2 + N_3$ independent trials were recorded, N_1, N_2 and N_3 being the number of walkers crossing valley 1, 2 and 3, respectively. The number of combinations leading to i trials in one of the three possible valleys reads,

$$\omega(i) = \sum_{j=0}^{N-i} \frac{N!}{i!j!(N-i-j)!} \qquad (1)$$

To know if one option is overrepresented in a cell compared to what a uniform random process would produce, we consider the number of occurrences of the most represented option in the cell, $M = \max(N_1, N_2, N_3)$. The number of combinations leading to a number of occurrences larger or equal to M is,

$$\Omega(M) = \sum_{i=M}^{N} \omega(i) = \sum_{i=M}^{N} \sum_{j=0}^{N-i} \frac{N!}{i!j!(N-i-j)!} \qquad (2)$$

The total number of different combinations is $\Omega(0) = \sum_{i=0}^{N} \omega(i) = 3^N$. Thus, the probability to obtain M or more walkers in one valley reads $p = \Omega(M)/\Omega(0)$. The choice of a valley is considered predictable if the probability for obtaining such a distribution is less than $p < 5\%$. Predictability is reported with gray cells in figure 4. Cells with white background are not predictable and cells with pink background have not been sufficiently tested ($N < 3$) to be sorted.

Several attractors are visible, where trajectories are biased to a given valley (e.g., black valley at $\phi \simeq \pi/6$ for low speed walkers). By contrast, there are regions where the choice of valley is very sensitive to parameters and initial conditions, e.g., for $\phi \gtrsim \pi$ at low speed. Surprisingly, bouncing phase reversals are more frequent in predictable regions of the parameter space.

C. Diffraction patterns

Figure 4 shows that trials are not evenly distributed in the parameter space. To provide a statistically meaningful analysis of the diffraction pattern, the full dataset is divided in 6 subsets gathering experiments with impact parameter $\phi \in [i\pi/3, (i+1)\pi/3]$, index $i = 0, ..., 5$.

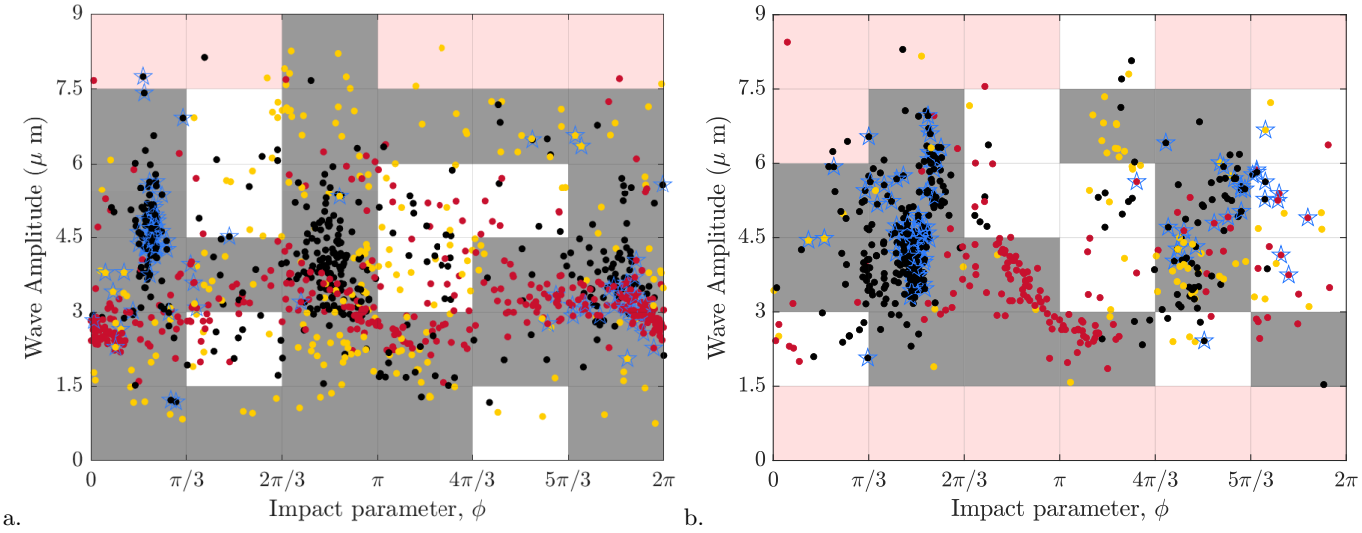

FIG. 4. Parameter space of the experiment: standing wave amplitude vs. impact parameter. The background color indicates the predictability of the choice of valley. Gray: the valley is predictable with a p-value less than 0.05. Pink: the predictability cannot be assessed since there are less than 3 data points. white: the valley is not predictable $p > 0.05$. The color of the symbols corresponds to the choice of valley. Red: top valley, Yellow: central valley, Black: bottom valley. Blue stars indicate the presence of a bouncing phase reversal. a. Low speed walkers ($v \in [11.5; 12.1]\text{mm s}^{-1}$). b. High speed walkers ($v \in [13.2; 13.8]\text{mm s}^{-1}$).

The Probability Distribution Function (PDF) of diffraction angles is calculated for each subset. Then these six PDFs are added with equal weight to generate the normalized distribution of angles, that would result from a uniform distribution of impact parameters.

This normalized distribution of diffraction angles is shown in figure 5 for low-speed droplets. The diffraction angles lie in the range [-40^o;+40^o] and their distribution is not uniform. Notably, the distribution exhibits depleted regions at around $\pm 15^o$. Considering different subsets based on speed, standing wave amplitude or both, always leads to a similar distribution with depleted regions.

The normalized angle distributions can be approximated by a symmetric three-peak function: $a\exp((x-b)^2/c^2) + d\exp(x^2/c^2) + f\exp((x+b)^2/c^2)$. Other symmetric distributions such as a five-peak distribution could have been considered. We finally opted for a three-peak distribution for simplicity. Fits are performed directly on the PDF considering a very large number of bins compared to the number of test to avoid binning dependent fitting. This fit assumes equal width c of all peaks, symmetric peak position $\pm b$ but possibly asymmetric peak amplitude, a, d, f. For the subset represented in figure 5, the peak positions are centered around 0^o, and $\pm 25^o$.

Figure 6 shows a scatter plot of the diffraction angle as a function of the wave amplitude, with colors according to the chosen valley. It clearly proves that the passage through a valley does not preclude the diffraction angle.

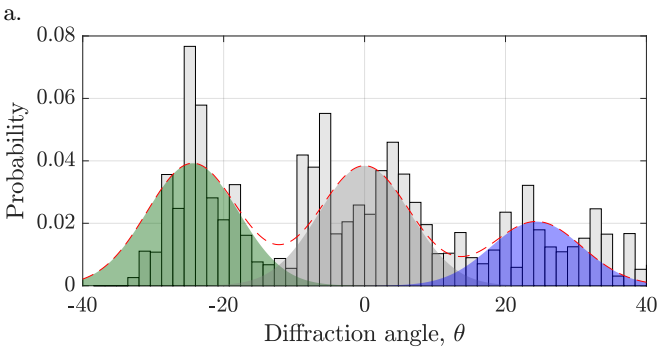

FIG. 5. a. Normalized distribution of diffraction angles (walker velocity, $v \in [11.5; 12.1]\text{mm s}^{-1}$, wave amplitude $A \in [0; 9.5]$ µm). The dashed red curve is a fit of the distribution by a sum of three gaussian functions centered in -25^o, 0^o and 25^o. Individual gaussian functions are represented with green, grey and blue shades.

D. Influence of wave amplitude

Normalized distributions of diffraction angles are shown in figure 7 for three different ranges of wave amplitude. Again, depleted regions are seen around $\pm 15^o$, and a 3-peak function can be fitted on the distributions.

The angle b of these peaks is plotted as a function of wave amplitude in figure 8a. It is more or less independent of the wave amplitude. The relative peaks amplitude are plotted in figure 8b, $|p_0| = d$ representing the probability to be in the central peak and $|p_1| = a + f$ the probability to be deviated in one of the two lateral peaks.

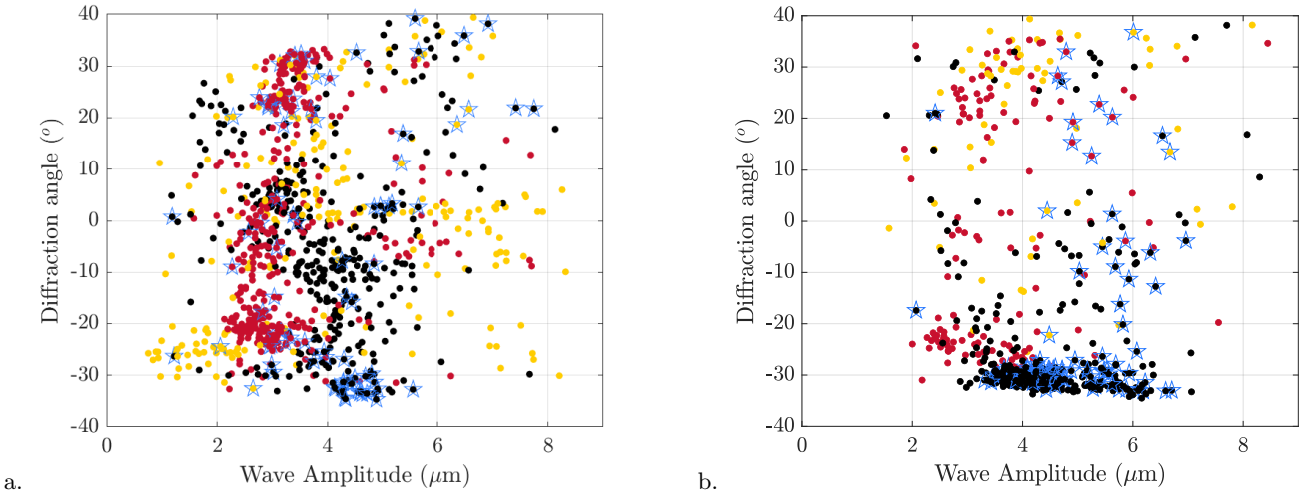

FIG. 6. Scatter plot of diffraction angle vs standing wave amplitude. The color of the symbols corresponds to the chosen valley (as in figure 3. Black: bottom valley. Red: top valley. Yellow: central valley. $A \in [0, 9.5]\mu$m). a. Walker velocity, $v \in [11.5;\ 12.1]\mathrm{mm\,s^{-1}}$ b. Walker velocity, $v \in [13.2;\ 13.8]\mathrm{mm\,s^{-1}}$.

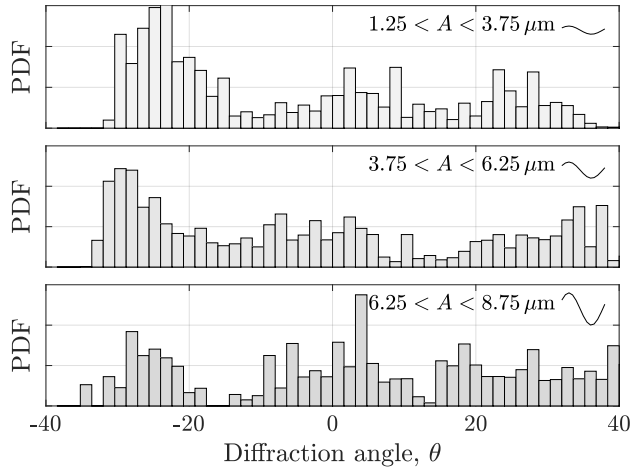

FIG. 7. Diffraction figure depending on wave amplitude. Top : $1.25 < A < 3.75\,\mu$m. Center: $3.75 < A < 6.25\,\mu$m. Bottom: $6.25 < A < 8.75\,\mu$m

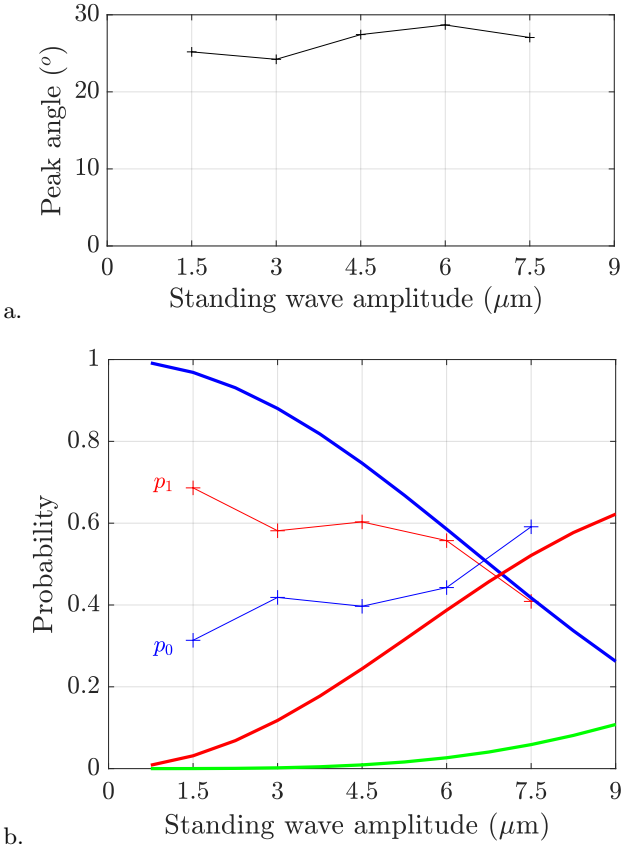

FIG. 8. a. Deviation angle of the distribution as a function of wave amplitude. b. probability to be in the central peak p_0 compared to the probability to be in one of the two first lateral peaks p_1. Thick solid lines indicates the quantum prediction with coefficient $C = 0.17\,\mu\mathrm{m}^{-1}$.

IV. DISCUSSION AND COMPARISON TO QUANTUM MECHANICS

The Kapitza-Dirac diffraction is the diffraction of quantum particles by an electro-magnetic standing wave, orthogonal to the beam of particles [29]. The present diffraction of walkers by a standing wave exhibits a similar configuration.

Batelaan [28] identified three main interactions between a quantum particle and an electromagnetic wave. (i) At low potential energy V and short interaction time τ, the particle is unaffected by the wave. (ii) At large V and short τ, the Kapitza-Dirac diffraction occurs with symmetric quantized peaks corresponding to a lateral

momentum of multiple of $2\hbar k$, where $\hbar$ is the Planck constant and k the wavenumber of the standing wave. The central peak is present only at sufficiently low V. (iii) At large V and long τ, the particle is in the channelling regime. The diffraction figure is symmetric with two major peaks of lateral momentum corresponding to several tens of $\hbar k$. In this work, walkers are observed in a regime that phenomenologically corresponds to the Kapitza-Dirac diffraction. In particular, the amplitude of the standing wave is of the same order of magnitude as the amplitude of the wave generated by the walker, which may be considered as a moderate V.

The diffraction figure obtained with walkers exhibits 3 peaks, similarly to the diffraction of sodium atoms by a standing wave of light at $V\tau/\hbar = 1.86$, test A4 from Gould *et al.* [30]. However similarity does not hold for analogy. Are the amplitudes of these three peaks evolving with variations of potential energy (i.e., variations of standing wave amplitude), in the same way for walkers and quantum particles?

According to the quantum prediction of Kapitza-Dirac diffraction, the probability to find a particle in the central peak is $J_0(V\tau/\hbar)^2$. The probability for the quantum particle to receive two quanta of momentum $\pm 2\hbar k$ is $J_1(V\tau/\hbar)^2$ [28].

The argument of the Bessel functions is not easily transferable to walking droplets as there is no strict equivalent for $\hbar$. Moreover, the equivalent of the wave potential V for walkers is also unclear as the interaction of a walker with a standing wave has not been investigated theoretically. To possibly draw an analogy, we consider that the potential of the interaction between the wave and the walking droplet is likely to be proportional to the standing wave amplitude only [38], namely, $V\tau/\hbar \equiv CA$, where C is a proportionality coefficient (the interaction time being similar for all walkers, speed variations being limited). We chose $C = 0.17\,\mu\text{m}^{-1}$ because three and only three peaks are observed. For $C \ll 0.17\,\mu\text{m}^{-1}$, only the first peak would be visible. For $C \gg 0.17\,\mu\text{m}^{-1}$, the quantum theory predicts more than 3 peaks. $C \simeq 0.17\,\mu\text{m}^{-1}$ is a reasonable value to obtain $p_1 > 0$ and $p_2 \simeq 0$.

This value is used to compare quantum predictions with experimental data on walkers in figure 8b (bins of $1.5\,\mu\text{m}$). The comparison is poor: the quantum prediction indicates a probability p_0 that decreases as the potential energy increases, while the opposite is observed in the present experiments with walkers.

Would walking droplets be better modeled with a newtonian model that does not consider the fast dynamics (time scale: shaking frequency) of wave-particle interaction? For a short interaction time, we can model the standing wave as a lateral force,

$$m\ddot{y} = \alpha A \cos\left(\frac{2\pi y}{\lambda_F}\right) .$$

The deviation angle after interaction,

$$\theta = \text{atan}\left(\sqrt{\frac{2\alpha A}{v_w^2}\sin\left(\frac{2\pi y}{\lambda_F}\right)}\right)$$

According to such classical interaction, the deviation angle corresponding to the lateral peaks varies as $\text{atan}(\sqrt{A})$. The experimental data from figure 8a do not support such variation with A: the peak angle is constant.

V. CONCLUSION

In this work, walkers sent normally towards a localized standing Faraday wave have been observed to cross this wave through three channels corresponding to adjacent wave troughs called valleys. Once the wave is crossed, the walkers resume a linear trajectory with a deflection angle with respect to the wave. This behavior is reminiscent of the Kapitza-Dirac diffraction of a quantum particle by an electromagnetic wave. The interaction of a walking droplet with a moderate standing wave is predictable in some regions of the parameter space.

The diffraction figure exhibits two depleted regions at around $\pm 15^o$, and was here fitted by a symmetric 3-peak distribution.

The interaction of walkers with moderate standing wave is reminiscent of the Kapitza-Dirac interaction, in the sense that the distribution of diffraction angles exhibits three peaks corresponding to preferential directions. However, the probability associated to these preferred diffraction angles does not vary with wave amplitude in the same way as for quantum particles. Thus, this experiment does not support a full analogy between the two systems in the considered range of parameters. This range is relatively narrow. A better match between the quantum prediction and walker diffraction experiments might be found in other sections of the parameter space.

Most experimental works on walkers are dealing with submerged obstacles that are challenging to model. The present experiment does not test the non-locality of walkers but only the way they interact with a standing wave. Nevertheless, this experiment is a first step toward testing the non-locality of walkers without submerged obstacles by creating an analogue to the Mach-Zehnder interferometer for walkers.

ACKNOWLEDGMENTS

The authors would like to thank John Bush for fruitful discussions and Herman Batelaan for his valuable advice on comparison between walkers and quantum particles. This work was financially supported by the FNRS Grant No. CHAR. RECH.-1.B423.18 (Tadrist L.). L.T. and T.G. designed the experiment. L.T. built and calibrated

the setup, acquired the data, then processed and analyzed them. L.T. and T.G. wrote the manuscript. Authors declare no competing interest.

DATA AVAILABILITY

The data that support the findings of this article are openly available [39].

[1] Y. Couder, S. Protiere, E. Fort, and A. Boudaoud, Walking and orbiting droplets, Nature **437**, 208 (2005).

[2] E. Fort, A. Eddi, A. Boudaoud, J. Moukhtar, and Y. Couder, Path-memory induced quantization of classical orbits, Proceedings of the National Academy of Sciences of the United States of America **107**, 17515 (2010).

[3] J. W. Bush, Y. Couder, T. Gilet, P. A. Milewski, and A. Nachbin, Introduction to focus issue on hydrodynamic quantum analogs, Chaos: An Interdisciplinary Journal of Nonlinear Science **28**, 096001 (2018).

[4] J. W. Bush and A. U. Oza, Hydrodynamic quantum analogs, Reports on Progress in Physics **84**, 017001 (2020).

[5] A. Eddi, J. Moukhtar, S. Perrard, E. Fort, and Y. Couder, Level splitting at macroscopic scale, Physical Review Letters **108**, 264503 (2012).

[6] D. M. Harris and J. W. M. Bush, Droplets walking in a rotating frame: from quantized orbits to multimodal statistics, Journal of Fluid Mechanics **739**, 444 (2014).

[7] A. U. Oza, D. M. Harris, R. R. Rosales, and J. W. M. Bush, Pilot-wave dynamics in a rotating frame: on the emergence of orbital quantization, Journal of Fluid Mechanics **744**, 404 (2014).

[8] M. Labousse, A. U. Oza, S. Perrard, and J. W. M. Bush, Pilot-wave dynamics in a harmonic potential: Quantization and stability of circular orbits, Physical Review E **93**, 033122 (2016).

[9] D. M. Harris, J. Moukhtar, E. Fort, Y. Couder, and J. W. M. Bush, Wavelike statistics from pilot-wave dynamics in a circular corral, Physical Review E **88**, 011001 (R) (2013).

[10] T. Gilet, Dynamics and statistics of wave-particle interactions in a confined geometry, Physical Review E **90**, 052917 (2014).

[11] T. Gilet, Quantumlike statistics of deterministic wave-particle interactions in a circular cavity, Physical Review E **93**, 042202 (2016).

[12] S. Perrard, M. Labousse, M. Miskin, E. Fort, and Y. Couder, Self-organization into quantized eigenstates of a classical wave-driven particle, Nature Communications **5**, 3219 (2014).

[13] M. Labousse, S. Perrard, Y. Couder, and E. Fort, Build-up of macroscopic eigenstates in a memory-based constrained system, New Journal of Physics **16**, 113027 (2014).

[14] K. Papatryfonos, M. Ruelle, C. Bourdiol, A. Nachbin, J. W. Bush, and M. Labousse, Hydrodynamic superradiance in wave-mediated cooperative tunneling, Communications Physics **5**, 1 (2022).

[15] K. Papatryfonos, L. Vervoort, A. Nachbin, M. Labousse, and J. W. Bush, Bell test in a classical pilot-wave system, arXiv preprint arXiv:2208.08940 (2022).

[16] Y. Couder and E. Fort, Single-particle diffraction and interference at a macroscopic scale, Physical Review Letters **97**, 154101 (2006).

[17] A. Andersen, J. Madsen, C. Reichelt, S. R. Ahl, B. Lautrup, C. Ellegaard, M. T. Levinsen, and T. Bohr, Double-slit experiment with single wave-driven particles and its relation to quantum mechanics, Physical Review E **92**, 013006 (2015).

[18] G. Pucci, D. M. Harris, L. M. Faria, and J. W. Bush, Walking droplets interacting with single and double slits, Journal of Fluid Mechanics **835**, 1136 (2018).

[19] L. Tadrist, J.-B. Shim, T. Gilet, and P. Schlagheck, Faraday instability and subthreshold faraday waves: surface waves emitted by walkers, Journal of Fluid Mechanics **848**, 906 (2018).

[20] C. Ellegaard and M. T. Levinsen, Interaction of wave-driven particles with slit structures, Physical Review E **102**, 023115 (2020).

[21] C. Ellegaard and M. T. Levinsen, Experimental investigation of walking drops: Wave field and interaction with slit structures, Physical Review E **109**, 035101 (2024).

[22] D. Darrow and J. W. Bush, Single-particle fraunhofer diffraction in a classical pilot-wave model, Physical Review Research **7**, 033288 (2025).

[23] S. Protiere, *Gouttes rebondissantes: une association onde-particule à échelle macroscopique*, Ph.D. thesis, Université Paris-Diderot-Paris VII (2007).

[24] G. Pucci, P. J. Sáenz, L. M. Faria, and J. W. M. Bush, Non-specular reflection of walking droplets, Journal of Fluid Mechanics **804**, R3 (2016).

[25] L. M. Faria, A model for faraday pilot waves over variable topography, Journal of Fluid Mechanics **811**, 51 (2017).

[26] M. Rode, J. Madsen, and A. Andersen, Wave fields in double-slit experiments with wave-driven droplets, Physical Review Fluids **4**, 104801 (2019).

[27] P. L. Kapitza and P. A. M. Dirac, The reflection of electrons from standing light waves, Mathematical Proceedings of the Cambridge Philosophical Society **29**, 297–300 (1933).

[28] H. Batelaan, The kapitza-dirac effect, Contemporary Physics **41**, 369 (2000).

[29] D. L. Freimund, K. Aflatooni, and H. Batelaan, Observation of the kapitza–dirac effect, Nature **413**, 142 (2001).

[30] P. L. Gould, G. A. Ruff, and D. E. Pritchard, Diffraction of atoms by light: The near-resonant kapitza-dirac effect, Phys. Rev. Lett. **56**, 827 (1986).

[31] B. K. Primkulov, D. J. Evans, V. Frumkin, P. J. Sáenz, and J. W. Bush, Diffraction of walking drops by a standing faraday wave, Physical Review Research **7**, 013226 (2025).
[32] J. Chen, J. G. Story, and R. G. Hulet, Evolution of atomic motion in an intense standing wave, Physical Review A **47**, 2128 (1993).
[33] N. Ionkin and D. M. Harris, Note: A versatile 3d-printed droplet-on-demand generator, Review of Scientific Instruments **89**, 116103 (2018).
[34] See movies in supplemental material https://doi.org/10.1103/tqyd-hs8b . ().
[35] N. Sampara and T. Gilet, Two-frequency forcing of droplet rebounds on a liquid bath, Physical Review E **94**, 053112 (2016).
[36] F. Moisy, M. Rabaud, and K. Salsac, A synthetic schlieren method for the measurement of the topography of a liquid interface, Experiments in Fluids **46**, 1021 (2009).
[37] L. Tadrist, N. Sampara, P. Schlagheck, and T. Gilet, Interaction of two walkers: Perturbed vertical dynamics as a source of chaos, Chaos: An Interdisciplinary Journal of Nonlinear Science **28**, 096113 (2018).
[38] J. Moláček and J. W. M. Bush, Drops walking on a vibrating bath: towards a hydrodynamic pilot-wave theory, Journal of Fluid Mechanics **727**, 612 (2013).
[39] Data are available in supplemental material https://doi.org/10.1103/tqyd-hs8b . ().

SUPPLEMENTARY INFORMATION

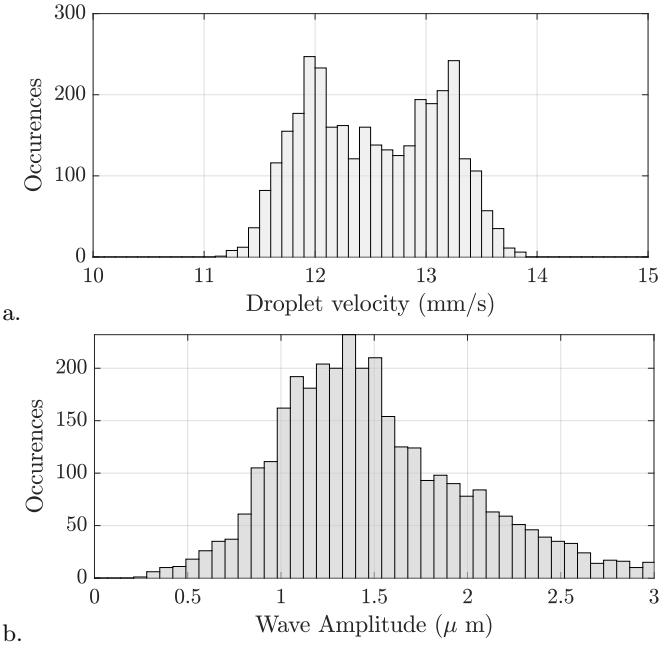

a.

b.

FIG. 9. a. Distribution of walkers speeds of the full data set. b. Distribution of Faraday wave Amplitudes of the full dataset.